

Bathymetry Estimation Using Machine Learning in the Ulleung Basin in the East Sea

Kwang Bae Kim,¹ Ji Sung Kim,^{2*} and Hong Sik Yun³

¹Department of Civil, Architectural, and Environmental System Engineering, Sungkyunkwan University,
2066 Seobu-ro, Jangan-gu, Suwon, Gyeonggi-do 16419, Republic of Korea

²School of Geography, University of Leeds, Woodhouse Lane, Leeds LS2 9JT, United Kingdom

³Interdisciplinary Program in Crisis, Disaster and Risk Management, Sungkyunkwan University,
2066 Seobu-ro, Jangan-gu, Suwon, Gyeonggi-do 16419, Republic of Korea

(Received April 3, 2023; accepted August 15, 2023)

Keywords: machine learning, Ulleung Basin, gravity–geologic method, satellite altimetry-derived free-air gravity anomalies, residual gravity anomalies

Accurate bathymetry estimation is made possible by combining depth data with free-air gravity anomalies on the sea surface recovered from the geoidal heights that are equivalent to the mean sea surface derived from satellite radar altimetry. The residual gravity anomalies that represent the short-wavelength effect are required to accurately estimate bathymetry by combining satellite altimetry-derived free-air gravity anomalies and shipborne data including depth and gravity anomalies. In this study, the optimized ensemble model of machine learning techniques was applied to the residual gravity anomalies to estimate bathymetry by the gravity–geologic method (GGM) from various geospatial information including shipborne depth, shipborne gravity anomalies, and satellite altimetry-derived free-air gravity anomalies, in the Ulleung Basin in the East Sea. From the results, the GGM bathymetry predicted using the optimized ensemble model of machine learning was improved by 32.3 m over the GGM bathymetry estimated using the original depth and gravity anomalies. The method presented in this study is for estimating deep-water bathymetry using machine learning, and it has been proven to have superior performance compared with conventional methods.

1. Introduction

Bathymetry mapping is important in understanding Earth's gravity field. Recently, various research studies have been performed to predict accurate bathymetry using shipborne data, including depth and gravity anomalies, by utilizing high-resolution satellite altimetry-derived free-air gravity anomalies.

Various machine learning technologies have also been developed and applied to each field of surveying. In bathymetry estimation in particular, research using machine learning technology has been actively conducted. In fact, many studies have revealed that machine learning is accurate and fast in comparison with conventional bathymetry measurement methods. Collin

*Corresponding author: e-mail: gyjki@leeds.ac.uk
<https://doi.org/10.18494/SAM4415>

and Hench⁽¹⁾ extracted spectra from very high resolution satellite images, formed neural bands through an artificial neural network, and estimated shallow-water bathymetry. In their study, the authors demonstrated that bathymetry estimation using machine learning is superior to conventional methods. Misra *et al.*⁽²⁾ extracted shallow-water bathymetry using multispectral images of satellites, similarly to Collin and Hench.⁽¹⁾ However, their study used a support vector machine (SVM) rather than an artificial neural network. A significant number of studies on bathymetry estimation in shallow areas using satellite imagery and artificial intelligence have been conducted since 2015.^(3–10) Most of these studies used multispectral images obtained from satellites but different machine learning methods. Owing to the characteristics of multispectral images, it is difficult to measure a large water depth, so these studies are limited to shallow target areas where the water depth is less than 40 m. Despite these various studies, it is difficult to find studies on the utility and performance of machine learning in deep-water bathymetry, unlike shallow-water bathymetry. In addition, because the characteristics of shallow water and deep water are different, it is not possible to judge that the utility and performance of machine learning in deep-water bathymetry are the same as those of shallow water. Therefore, it is necessary to apply machine learning in deep-water bathymetry and understand its performance. To meet this demand, we used machine learning in deep-water bathymetry and determined its utility and performance. Machine learning techniques for measuring bathymetry are as diverse as the studies. For example, regression,^(6,9) artificial neural network,^(1,4,11) and SVM^(2,5–7,10,12,13) are common among various machine learning methods. All these methods yield better performance than the conventional simple interpolation but their performance varies depending on the study. Among them, the decision tree appears to yield the best performance. Sagawa *et al.*⁽⁵⁾ and Susa⁽¹³⁾ have demonstrated the capacity of random forest in bathymetry estimation. Alevizos⁽⁶⁾ showed that random forest was superior to kappa nearest neighbor (KNN) and multiple linear regression analyses in bathymetry estimation. Furthermore, Tonion *et al.*⁽⁷⁾ demonstrated that random forest performed better than SVM in bathymetry estimation. Similarly, Eugenio *et al.*⁽¹⁰⁾ and Moran *et al.*⁽¹²⁾ both showed that decision tree is more suitable for bathymetry estimation than KNN and SVM. Considering these trends, it is necessary to apply various machine learning techniques and determine their suitability in this study.

The purpose of this study is to evaluate the accuracy of bathymetry grid data generated by the gravity–geologic method (GGM) using depth and gravity anomalies predicted using the optimized machine learning model, determined from various machine learning techniques, in the Ulleung Basin in the East Sea. To assess the accuracy, the bathymetry grid data generated using the optimized machine learning model were compared with the two global bathymetry grid data obtained using the global topography model (V19.1) of Scripps Institution of Oceanography (SIO, <http://www.sio.ucsd.edu>), University of California at San Diego⁽¹⁴⁾ and the 1 × 1 arc-minute Earth topographical database 1 (ETOPO1) model.⁽¹⁵⁾

2. Methods

2.1 Prediction of depth and gravity anomalies by machine learning

As described in the introduction, machine learning methods for bathymetry include regression analysis, SVM, the decision tree, and artificial neural networks. The superiority of the decision tree in bathymetry has been proven in numerous studies.^(5–7,10,12,13) However, since most of the above studies are aimed at shallow bathymetry, it cannot be assured that the decision tree can yield excellent performance even in deep-water bathymetry. Therefore, in this study, we tried to predict water depth and gravity anomalies using the method with the highest performance after analyzing performance using regression analysis, SVM, the decision tree, and artificial neural networks.

The regression models used in this study are linear, interactive, robust linear, and stepwise linear models. Linear regression is a simple first-order linear model, whereas interactive regression is a regression analysis method that considers the correlation between longitude and latitude, which are input values. Robust linear regression can detect and remove outliers in advance to resolve the sensitivity of outliers for linear regression. Stepwise linear regression refers to a regression method that performs three steps: forward selection, backward elimination, and bidirectional elimination to prevent overfitting.

SVM is one of the machine learning techniques suitable for classification using kernel functions. The kernel functions used in this study are a linear function, a quadratic function, a cubic function, and Gaussian functions. The Gaussian functions used have three parameters: σ , 4σ , and $1/4\sigma$. In addition, SVM, which can be optimized using a Bayesian function, was used.

In this study, we also used three decision tree methods: the bagging tree, also called random forest, the boosting tree, and an optimized ensemble. Since the technology has already proven its excellence, we also examined if these methods demonstrate excellent performance. The decision tree, like SVM, was used in this study by additionally creating a model that can be optimized using a Bayesian function, in addition to the bagging tree and boosting tree. The artificial neural network model adopts the Bayesian function for optimization from a neural network with three hidden layers that take latitude and longitude as input values.

To evaluate the performance of each technique and select a model suitable for bathymetry estimation, the root mean square error (*RMSE*), coefficient of determination (R^2), mean square error (*MSE*), and mean absolute error (*MAE*) were used in the validation set and the test set, respectively. Validation was performed by five fold cross-validation, and the test set separated 10% of the total data that was excluded from the training data.

2.2 Bathymetry prediction by GGM

The GGM for bathymetry prediction using satellite altimetry-derived free-air gravity anomalies has been performed in several studies.^(16–19) The satellite altimetry-derived free-air gravity anomalies can be used to fill gaps by computing the topographic effects in the off-tracks between the shipborne depth measurements in GGM.⁽¹⁶⁾

The observed gravity (g_{obs}) is made up of residual gravity (g_{short}) and regional gravity (g_{long}). As shown in Fig. 1, the residual gravity $g_{short}^{ML}(j)$ and the regional gravity $g_{long}^{ML}(j)$ from both depth estimation [$d^{ML}(j)$] and gravity anomalies estimation [$g^{ML}(j)$] using the optimized machine learning model at the shipborne measured point j were generated. The regional gravity $g_{long}^{ML}(j)$ at the points of measured depth j was calculated by subtracting the residual gravity $g_{short}^{ML}(j)$ that represented the effect of the seafloor bedrock from the observed gravity $g_{obs}^{ML}(j)$.

The regional gravity $g_{long}^{ML}(i)$ at the points of unmeasured depth i can be estimated by gridding the regional gravity $g_{long}^{ML}(j)$ at the points of measured depth j . The residual gravity $g_{short}^{ML}(i)$ for predicting the depth between the sea surface and the seafloor bedrock at the points of unmeasured depth i was estimated by eliminating the regional gravity $g_{long}^{ML}(i)$ from $g_{obs}(i)$ that is SAFAGAs (g^{sat}) in the following equation. SAFAGAs represent the satellite altimetry-derived free-air gravity anomalies.

$$g_{short}^{ML}(i) = 2\pi G(\Delta\rho)(d(i) - D^{ML}) \tag{1}$$

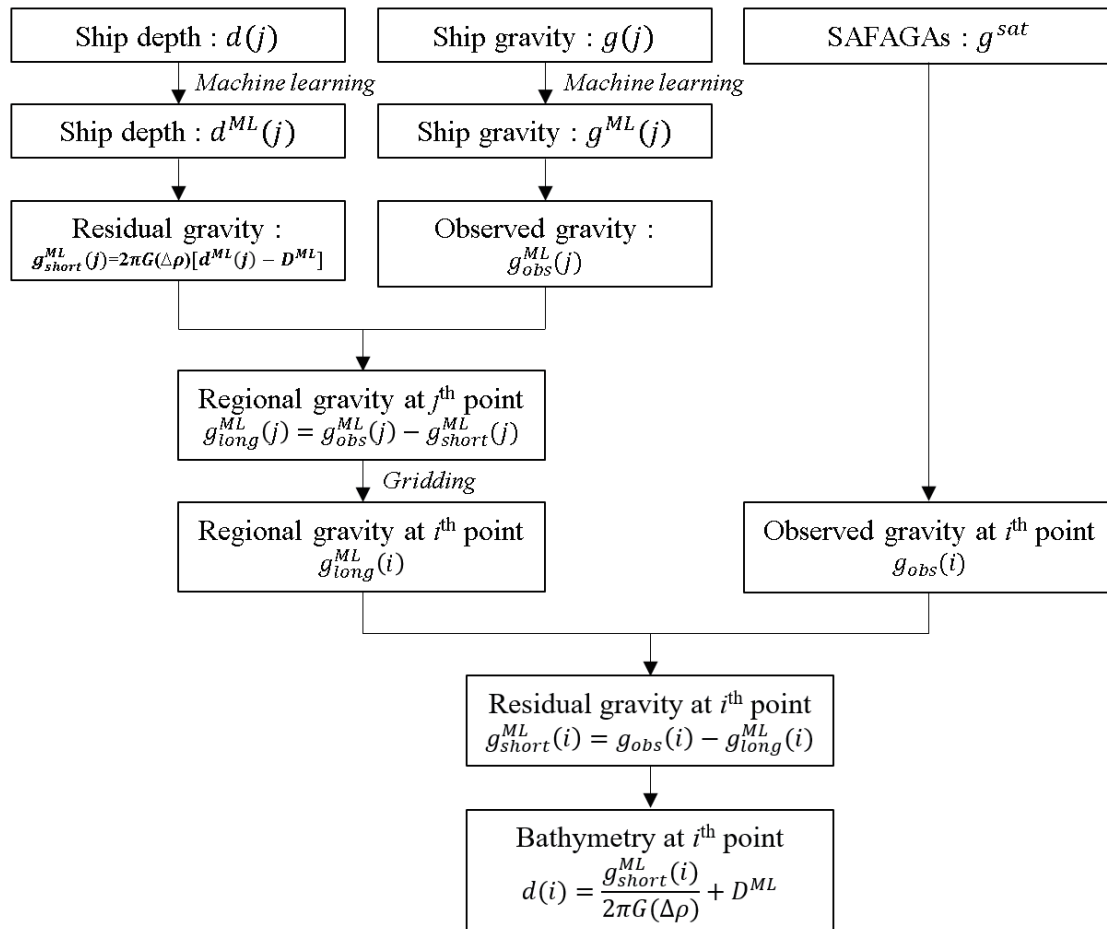


Fig. 1. Bathymetry estimation using GGM and machine learning.

The rearranged residual gravity $g_{short}^{ML}(i)$ at the points of unmeasured depth i was applied to predict bathymetry $d(i)$ in this study. In Fig. 1, G is the gravitational constant, $6.672 \times 10^{-8} \text{ cm}^3 \cdot \text{g}^{-1} \cdot \text{s}^{-2}$; $\Delta\rho$ is the density contrast (1.67 g/cm^3) between seawater (1.03 g/cm^3) and the seafloor bedrock (2.70 g/cm^3); D^{ML} is the deepest depth at a reference datum (m) using the optimized machine learning model at measured point j .

3. Results and Discussion

3.1 Determination of optimized machine learning model for predicting depth and gravity anomalies

In this study, we implemented bathymetry estimation using the optimized machine learning model in the Ulleung Basin in the East Sea, which was selected as the study area ($36\text{--}39^\circ\text{N}$, $130\text{--}133^\circ\text{E}$) denoted by the red box in Fig. 2(a). Figure 2(b) shows 247856 shipborne measurement locations, provided by the National Centers for Environmental Information (NCEI, <https://www.ncei.noaa.gov>), the National Oceanic and Atmospheric Administration (NOAA, <http://www.noaa.gov>), and the Korea Hydrographic and Oceanographic Agency (KHOA, <http://www.khoa.go.kr>), used for both shipborne depth estimation and shipborne gravity anomalies estimation using the optimized machine learning model. The 1 arc-minute satellite altimetry-derived free-air gravity anomalies (V29.1) obtained from Scripps Institution of Oceanography⁽¹⁴⁾ are superimposed as a background in Fig. 2(b).

To determine the machine learning model optimized for this study, $RMSE$, R^2 , MSE , and MAE in the validation set and test set were compared as described in the research methodology. The lower the $RMSE$, MSE , and MAE are, the better the performance becomes, with higher R^2 also yielding better performance.

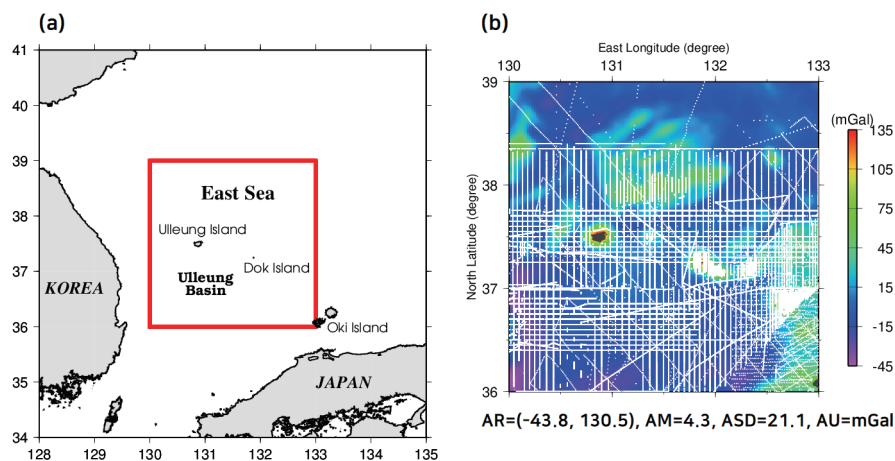


Fig. 2. (Color online) (a) Location map of study area (red box) and (b) 247856 shipborne measurement locations and satellite altimetry-derived free-air gravity anomalies⁽²⁰⁾ as a background. The attributes listed for this map include the amplitude range (AR = minimum and maximum values), amplitude mean (AM), amplitude standard deviation (ASD), and amplitude unit (AU).

In both shipborne depth estimation and shipborne gravity anomalies estimation, all models showed similar performances as presented in Tables 1 and 2. The performances yielded appear to be credible because indicators representing performance of each technique were similar in validation and testing. In the case of regression analysis, R^2 is less than 0.30 in both cases where depth and gravity anomalies are used. Therefore, it can be judged that regression analysis is not a suitable method for estimating depth and gravity anomalies. In the case of SVM, the performance varies depending on the kernel function, but when linear, quadratic, and cubic kernel functions are used, all coefficients of determination are less than 0.50. This means that

Table 1
Shipborne depth estimation performance for each machine learning model.

Machine learning model	Validation				Test			
	<i>RMSE</i>	R^2	<i>MSE</i>	<i>MAE</i>	<i>RMSE</i>	R^2	<i>MSE</i>	<i>MAE</i>
Linear regression	581.36	0.16	337980	478.72	580.06	0.16	336470	477.42
Interactive regression	541.61	0.27	293350	457.61	542.02	0.27	293780	458.01
Robust linear regression	582.46	0.15	339260	471.03	581.01	0.16	337570	469.55
Stepwise linear regression	541.61	0.27	293350	457.61	542.02	0.27	293780	458.01
Linear SVM	595.43	0.12	354540	459.58	594.47	0.12	35340	457.81
Quadratic SVM	513.02	0.34	263180	347.92	512.86	0.34	263020	348.80
Cubic SVM	454.67	0.48	206720	315.11	458.80	0.47	210500	325.16
Fine Gaussian SVM	124.37	0.96	15469	73.51	118.28	0.97	13990	71.25
Medium Gaussian SVM	291.76	0.79	85125	167.73	285.59	0.80	81560	164.25
Coarse Gaussian SVM	432.27	0.53	186860	291.38	429.00	0.54	184040	289.74
Optimization SVM	169.35	0.93	28679	82.53	160.18	0.94	25659	78.56
Boosting tree	297.75	0.80	78261	215.19	281.88	0.80	79455	217.77
Bagging tree	35.05	1.00	1228	16.66	29.52	1.00	872	15.67
Optimization ensemble	29.88	1.00	893	13.91	24.81	1.00	616	13.56
Optimization neural network	129.94	0.96	16885	78.41	101.27	0.97	10256	60.90

Table 2
Shipborne gravity anomalies estimation performance for each machine learning model.

Machine learning model	Validation				Test			
	<i>RMSE</i>	R^2	<i>MSE</i>	<i>MAE</i>	<i>RMSE</i>	R^2	<i>MSE</i>	<i>MAE</i>
Linear regression	23.34	0.24	544.89	15.71	23.25	0.25	540.45	15.73
Interactive regression	22.57	0.29	509.42	15.53	22.50	0.29	506.08	15.56
Robust linear regression	23.71	0.22	561.95	15.27	23.56	0.23	555.14	15.25
Stepwise linear regression	22.57	0.29	509.42	15.53	22.50	0.29	506.08	15.56
Linear SVM	23.58	0.23	555.95	15.23	23.43	0.23	548.88	15.21
Quadratic SVM	22.64	0.29	512.59	14.83	22.51	0.29	506.67	14.81
Cubic SVM	22.19	0.31	492.59	13.66	22.17	0.31	491.70	13.66
Fine Gaussian SVM	6.58	0.94	43.28	3.85	6.35	0.94	40.36	3.76
Medium Gaussian SVM	17.38	0.58	301.97	10.01	17.05	0.59	291.11	9.81
Coarse Gaussian SVM	21.88	0.33	478.77	13.38	21.74	0.34	472.47	13.27
Optimization SVM	26.80	0.00	718.22	20.36	26.78	0.00	716.98	20.41
Boosting tree	13.45	0.75	180.95	9.19	13.47	0.75	181.51	9.28
Bagging tree	1.77	1.00	3.13	0.95	1.71	1.00	2.93	0.90
Optimization ensemble	1.40	1.00	1.95	0.72	1.45	1.00	2.10	0.71
Optimization neural network	5.72	0.95	32.70	3.84	4.88	0.97	23.77	3.24

SVM using the polynomial kernel function is not appropriate for this study. On the other hand, when using the Gaussian function as a kernel function, R^2 increases to 0.9 or more.

As in the preceding cases,^(5–7,10,12,13) the decision tree models show overwhelmingly superior performance compared with other techniques. With the bagging tree, R^2 is close to 1.00, and $RMSE$, MSE , and MAE are sharply reduced compared with those of other techniques. Furthermore, when the decision tree is optimized using the Bayesian function, improved results can be seen compared with those of the general bagging tree. The artificial neural network optimized using the Bayesian function also appears to have R^2 of 0.95 or higher.

From the above results, the optimized ensemble model using hyper parameters is deemed suitable for achieving the purpose of this study. It shows significant performance compared with other methods in terms of both depth and gravity anomalies estimation. Considering the error indicators and R^2 close to 1.00, the data estimated using the optimized ensemble model can be considered as highly reliable.

3.2 Evaluation of bathymetry grid data prediction using the optimized machine learning model

In this study, the two bathymetry grid data, GGM (ML) and GGM, applied to GGM using a density contrast of 1.67 g/cm^3 were generated using the depth and gravity anomalies predicted with the optimized ensemble model of machine learning and the original shipborne depth and gravity anomalies, respectively. Bathymetry grid data of 1 arc-minute obtained by GGM (ML) using the optimized ensemble, GGM, SIO (V19.1), and ETOPO1 are shown in Fig. 3. The results of statistical comparisons are summarized in Table 3. The GGM (ML) grid data indicate high correlation coefficients of 0.9867, 0.9853, and 0.9805 with GGM, SIO (V19.1), and ETOPO1, respectively. The GGM grid data also show correlation coefficients of 0.9749 and 0.9711 with SIO (V19.1) and ETOPO1, respectively.

Maps of point-by-point differences between the bathymetry grid data are shown in Fig. 4, and Table 4 summarizes the relevant statistics. GGM (ML) grid data estimated using the optimized

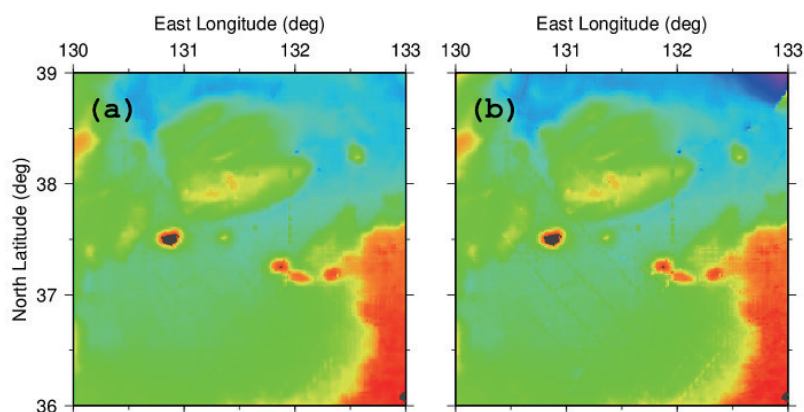


Fig. 3. (Color online) Four sets of bathymetry grid data obtained by (a) GGM (ML), (b) GGM, (c) SIO (V19.1), and (d) ETOPO1.

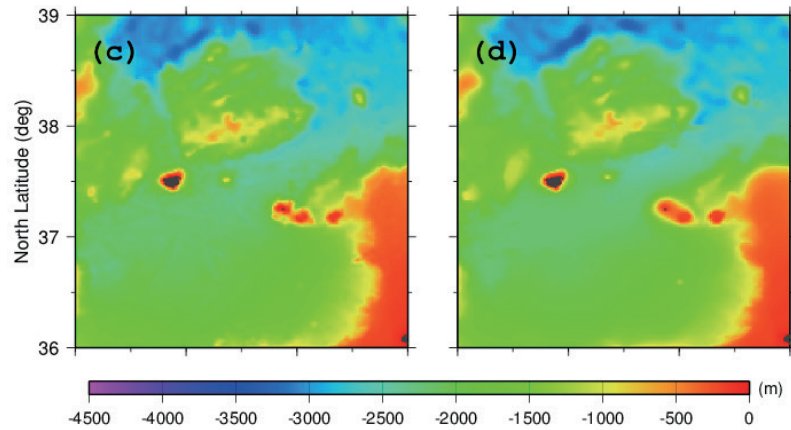


Fig. 3. (Continued) (Color online) Four sets of bathymetry grid data obtained by (a) GGM (ML), (b) GGM, (c) SIO (V19.1), and (d) ETOPO1.

Table 3

Results of statistical comparisons between bathymetry grid data: GGM (ML), GGM, SIO (V19.1), and ETOPO1 in the study area (unit: meter).

	Min	Max	Mean	Std dev
GGM (ML)	-3087.0	0.0	-1879.7	679.8
GGM	-4347.6	0.0	-1889.5	712.1
SIO (V19.1)	-3231.2	0.0	-1865.1	712.0
ETOPO1	-3427.0	0.0	-1849.4	707.0

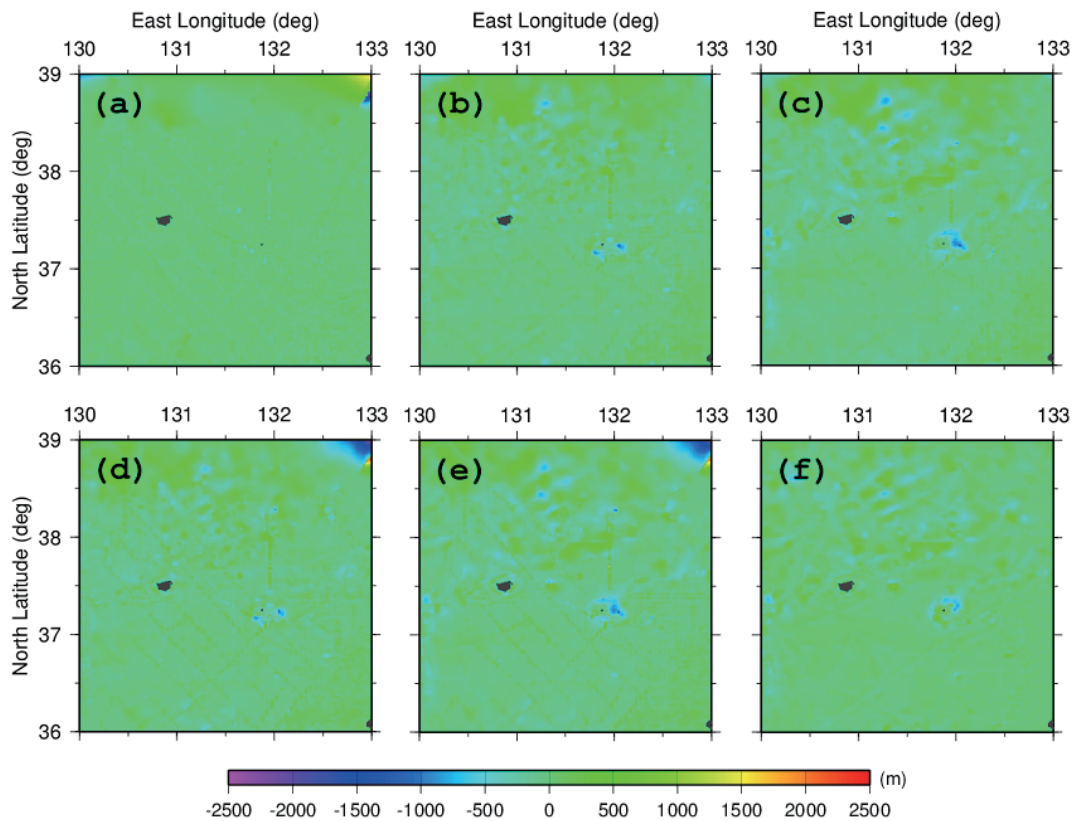


Fig. 4. (Color online) Differences between four sets of bathymetry grid data obtained by (a) GGM (ML)–GGM, (b) GGM (ML)–SIO (V19.1) (c) GGM (ML)–ETOPO1, (d) GGM–SIO (V19.1), (e) GGM–ETOPO1, and (f) SIO (V19.1)–ETOPO1.

Table 4

Statistics of the differences between four bathymetry grid data: GGM (ML), GGM, SIO (V19.1), and ETOPO1 (unit: meter).

	Min	Max	Mean	Std dev
GGM (ML)–GGM	–2516.0	1629.1	9.8	118.0
GGM (ML)–SIO (V19.1)	–1260.8	926.3	–14.7	123.6
GGM (ML)–ETOPO1	–1298.2	946.1	–30.4	139.5
GGM–SIO (V19.1)	–2193.2	2466.0	–24.5	159.4
GGM–ETOPO1	–2083.7	2485.2	–40.2	170.6
SIO (V19.1)–ETOPO1	–822.3	943.5	–15.8	99.1

ensemble model of machine learning were in better agreement than GGM grid data estimated using the original depth and gravity anomalies in comparison with SIO (V19.1) and ETOPO1. In Figs. 4(d) and 4(e), the depth differences are more than ± 1500 m in the upper right corner. These large differences in the upper right corner are caused by the overestimated GGM bathymetry in the upper right corner areas of Fig. 3(b), where there are no shipborne data as shown in Fig. 2(b). The estimated depth and gravity anomalies in the upper right corner using the optimized ensemble model of machine learning were effectively utilized to generate GGM (ML) grid data in comparison with GGM grid data. These results may indicate that the GGM (ML) grid data estimated using the optimized ensemble model of machine learning has better bathymetry compared with the GGM grid data.

According to the summarized statistics in Table 4, the standard deviations of differences of bathymetry grid data between GGM (ML) and SIO (V19.1), and between GGM and SIO (V19.1) are 123.6 m and 159.4 m, respectively. In addition, the standard deviations of differences of bathymetry grid data between GGM (ML) and ETOPO1, and between GGM and ETOPO1 are 139.5 m and 170.6 m, respectively. Thus, the GGM grid data estimated using the optimized ensemble model of machine learning can effectively predict bathymetry by utilizing the topographic effects in the off-tracks extracted from the satellite altimetry-derived free-air gravity anomalies in the Ulleung Basin in the East Sea.

To evaluate the accuracy of the GGM (ML) grid data predicted using the optimized ensemble model of machine learning and GGM, the bathymetry grid was interpolated into the 247856 shipborne locations, which are represented by the white dots in Fig. 2(b). Figure 5 shows the depth differences (a) between GGM (ML) and SHIP and (b) between GGM and SHIP at 247856 shipborne depth locations. Although the mean of the depth differences between GGM (ML) and SHIP is larger than that of the depth differences between GGM and SHIP in Table 5, the standard deviation of the depth differences between GGM (ML) and SHIP is smaller than that of the depth differences between GGM and SHIP. These results may indicate that the GGM (ML) grid data predicted using the optimized ensemble model of machine learning can generate accurately bathymetry in the Ulleung Basin in the East Sea.

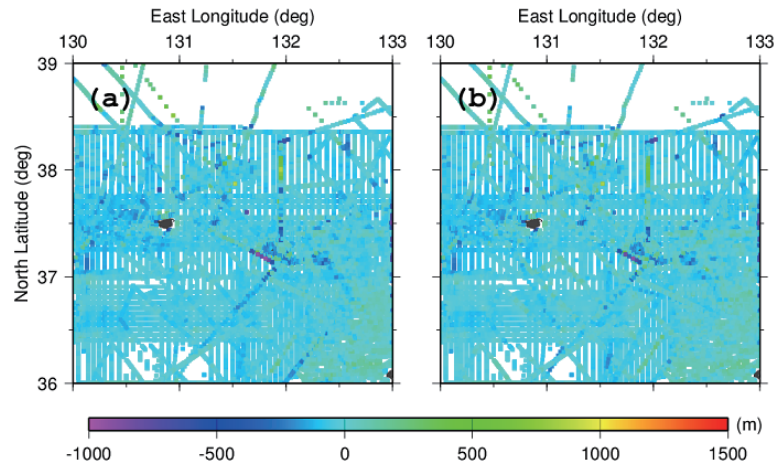


Fig. 5. (Color online) Differences in bathymetry at 247856 shipborne locations between (a) GGM (ML) and SHIP and (b) GGM and SHIP.

Table 5

Statistics of depth differences at 247856 shipborne locations between GGM (ML) and SHIP and between GGM and SHIP (Unit: meter).

	Min	Max	Mean	Std dev
GGM (ML)	-1333.9	2198.2	-52.4	70.6
GGM	-1315.2	2092.1	-49.7	72.0

4. Conclusions

In this study, we estimated the bathymetry in the Ulleung Basin in the East Sea by applying GGM to depth and gravity anomalies predicted using the optimized ensemble model of machine learning. The GGM bathymetry predicted using the optimized ensemble model of machine learning presents an improvement of 32.3 m in standard deviation (679.8 m in Table 3) in comparison with the standard deviation (712.1 m) of the GGM bathymetry estimated using the original depth and gravity anomalies. When the density contrast (1.67 g/cm^3) was utilized, the accuracy of the GGM bathymetry estimation using the optimized machine learning model was 70.6 m in comparison with shipborne depth values in the Ulleung Basin in the East Sea.

The method presented in this study is for estimating deep-water bathymetry using machine learning, and it has been proven to have superior performance compared with conventional methods. Therefore, with regards to contribution to the sensing field, the methodology of this study not only improved the accuracy of bathymetry but also increased the utilization of the sensors in that it improved the accuracy of data obtained from each sensor.

In a future study, we will determine whether a tuning density contrast larger than 1.67 g/cm^3 , or the theoretical density contrast between seawater and the seafloor bedrock, can improve the accuracy of bathymetry grid data when enough shipborne depth data become available.

Acknowledgments

This research was supported by the Basic Science Research Program through the National Research Foundation of Korea (NRF) funded by the Ministry of Education (NRF-2022R111A1A01053609). This work was supported by the Korea Environmental Industry and Technology Institute (KEITI) through the Environmental R and D Project on the Disaster Prevention of Environmental Facilities Program funded by the Korea Ministry of Environment (MOE) (No. 2020002860001). The authors also thank the National Centers for Environmental Information, the National Oceanic and Atmospheric Administration and the Korea Hydrographic and Oceanographic Agency for providing the shipborne depth data.

References

- 1 A. Collin and J. Hench: Proc. 2015 Int. Council for the Exploration of the Sea (ICES, 2015) N24.
- 2 A. Misra, Z. Vojinovic, B. Ramakrishnan, A. Luijendijk, and R. Ranasinghe: *Int. J. Remote Sens.* **39** (2018) 4431.
- 3 P. Agrafiotis, D. Skarlatos, A. Georgopoulos, and K. Karantzalos: Proc. 2019 Int. Arch. Photogramm. Remote Sens. Spatial Inf. Sci. (2019) 9. <https://doi.org/10.5194/isprs-archives-XLII-2-W10-9-2019>
- 4 K. Dickens and A. Armstrong: *SMU Data Sci. Rev.* **2** (2019) Article 4.
- 5 T. Sagawa, Y. Yamashita, T. Okumura, and T. Yamanokuchi: *Remote Sens.* **11** (2019) 1155. <https://doi.org/10.3390/rs11101155>
- 6 E. Alevizos: *Remote Sens.* **12** (2020) 3489. <https://doi.org/10.3390/rs12213489>
- 7 F. Tonion, F. Pirotti, G. Faina, and D. Paltrinieri: Proc. 2020 ISPRS Ann. Photogramm. Remote Sens. Spatial Inf. Sci. (XXIV ISPRS Congress, 2020) 565. <https://doi.org/10.5194/isprs-annals-V-3-2020-565-2020>
- 8 V. V. Surisetty, C. Venkateswarlu, B. Gireesh, K. V. S. R. Prasad, and R. Sharma: *Adv. Space Res.* **68** (2021) 3342. <https://doi.org/10.1016/j.asr.2021.06.034>
- 9 A. Ashphaq, P. Srivastava, and D. Mitra: *Reg. Stud. Mar. Sci.* **56** (2022) 102678. <https://doi.org/10.1016/j.rsma.2022.102678>
- 10 F. Eugenio, J. Marcello, A. Mederos-Barrera, and F. Marques: *IEEE Trans. Geosci. Remote Sens.* **60** (2022) 5407614. <https://doi.org/10.1109/TGRS.2021.3135462>
- 11 M. Al Najjar, G. Thoumyre, E. W. J. Bergsma, R. Almar, R. Benschila, and D. G. Wilson: *Mach. Learn.* **112** (2021) 1107. <https://doi.org/10.1007/s10994-021-05977-w>
- 12 N. Moran, B. Stringer, B. Lin, and Md. T. Hoque: *Deep Sea Res. Pt. I* **185** (2022) 103788. <https://doi.org/10.1016/j.dsr.2022.103788>
- 13 T. Susa: *Mar. Geod.* **45** (2022) 435. <https://doi.org/10.1080/01490419.2022.2064572>
- 14 W. H. F. Smith and D. T. Sandwell: *Science* **277** (1997) 1956. <https://doi.org/10.1126/science.277.5334.1956>
- 15 C. Amante and B. W. Eakins: ETOPO1 1 Arc-Minute Global Relief Model: Proc. Data Sources and Analysis (NOAA, 2009) 19.
- 16 K. B. Kim, Y.-S. Hsiao, J. W. Kim, B. Y. Lee, Y. K. Kwon, and C. H. Kim: *Mar. Geophys. Res.* **31** (2010) 285. <https://doi.org/10.1007/s11001-010-9110-0>
- 17 K. B. Kim and C. K. Lee: *J. Korean Soc. Surv. Geod. Photogram. Cartography* **33** (2015) 181. <https://doi.org/10.7848/ksgpc.2015.33.3.181>
- 18 K. B. Kim and H. S. Yun: *KSCE J. Civ. Eng.* **22** (2018) 2560. <https://doi.org/10.1007/s12205-017-0487-z>
- 19 K. B. Kim and H. S. Yun: *J. Coastal Res.* **114** (2021) 390. <https://doi.org/10.2112/JCR-S114-079.1>
- 20 D. T. Sandwell, R. D. Müller, W. H. F. Smith, E. Garcia, and R. Francis: *Science* **346** (2014) 65. <https://doi.org/10.1126/science.1258213>

About the Authors



Kwang Bae Kim received his B.S. and M.S. degrees from Sungkyunkwan University, Korea, in 1993 and 1996, respectively. He received his M.S. degree from Ohio State University, USA, in 2001 and Ph.D. degree from Kunsan National University, Korea, in 2016. Since 2016, he has been a research professor at Sungkyunkwan University. His research interests are in satellite geodesy and bathymetry mapping. (kbkim929@skku.edu)



Ji Sung Kim received his B.S. and M.S. degrees from Sungkyunkwan University, Korea, in 2013 and 2015, respectively. He received his Ph.D. degree from the Department of Civil, Architectural, and Environmental System Engineering at Sungkyunkwan University in 2021. His research interests are in remote sensing and earth science. (gyjki@leeds.ac.uk)



Hong Sik Yun received his B.S. and M.S. degrees from Sungkyunkwan University, Korea, in 1984 and 1987, respectively. He received his Ph.D. degree from the Technical University of Budapest, Hungary, in 1995. Since 1999, he has been a professor at Sungkyunkwan University. His research interests are in satellite geodesy, GNSS positioning, and geoid modeling. (yoons@skku.edu)